Nonequilibrium solidification in Fe-C-Al-Mn steel welds

S. S. Babu[*], J. W. Elmer[**], S. A. David[*] and M. Quintana[†]

[*]Metals and Ceramic Division, Oak Ridge National Laboratory, Oak Ridge, TN 37831

[**]Lawrence Livermore National Laboratory, Livermore, CA 94550

[†] The Lincoln Electric Company, Cleveland, Ohio 44117

Introduction

Previous research focused on inclusion and microstructural evolution in self-shielded Fe-C-Al-Mn flux-cored arc welds [1, 2]. Microstructural characterization of welds with aluminum concentration less than 1 wt.% showed the presence of aluminum oxide and titanium carbonitride inclusions and classical α-ferrite microstructure that forms from 100% austenite. In welds with aluminum concentration greater than 1.5 wt.%, aluminum nitride inclusions were present and the oxide inclusions were absent. In addition, the primary solidification through δ-ferrite phase was observed. On cooling further, incomplete transformation of δ-ferrite to austenite takes place. As a result, the final microstructure of high-aluminum welds contained columnar δ-ferrite. These microstructures were successfully predicted with computational thermodynamic and kinetic models [1, 2]. To evaluate these models, the phase transformations that occur in the heat-affected-zone (HAZ) and the weld metal (WM) region of the high-aluminum gas-tungsten arc spot weld were monitored with *in-situ* time-resolved X-ray diffraction (TRXRD) technique.

Experimental

TRXRD measurements were performed on a 31-pole wiggler 10-2 beam line [3] at Stanford Synchrotron Radiation Laboratory. The synchrotron white beam emerging from the 31-pole wiggler was focused by a toroidal mirror and was then mono-chromatized with a double Si (111) crystal. A 730-μm-diam pinhole was used to achieve the time resolution necessary to capture phase transformations during the rapid thermal cycling of transient stationary spot-welds [4]. This setup yielded a beam flux on the sample of 10^{10} to 10^{11} photons/s, as determined experimentally using an ion chamber downstream from the pinhole. The diffraction intensities at various 2θ positions were monitored continuously and in real time using a 5 cm-long photodiode array covering a 2θ range of approximately 30°. The experimental setup is shown in Fig. 1.

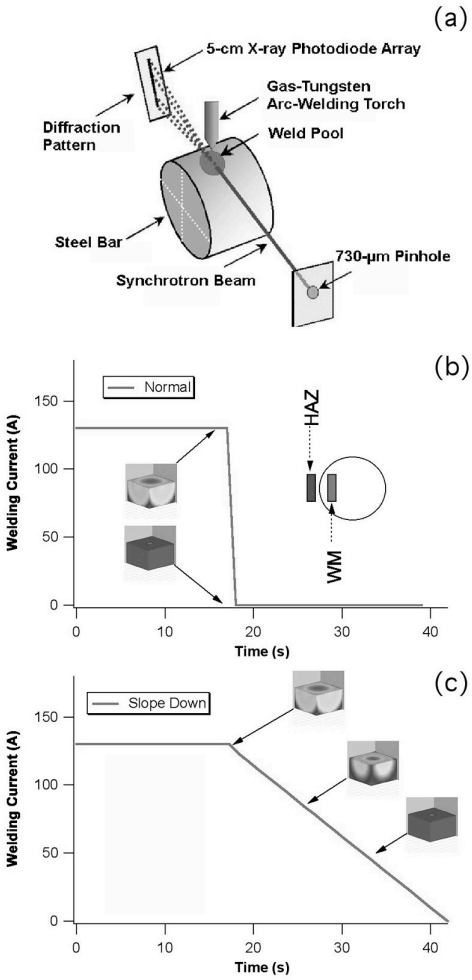

Fig. 1 (a) Experimental setup for TRXRD experiments, (b) schematic representation of static weld experiment where the arc was extinguished instantaneously, and (c) slope-down experiment where the arc current was reduced slowly from maximum value to zero in 25 s.

In general, three body-centered cubic (bcc) ferrite peaks [(110), (200), and (211)] and three face-centered cubic (fcc) austenite peaks [(111), (200), and (220)] were identified. The diffraction spectra were collected at 0.05-s time intervals during transient heating and cooling of stationary arc welds.

A 4-inch diameter cylinder was produced by a surface cladding using a self-shielded flux-cored arc-welding process on a mild steel bar. During surface cladding, care was taken to avoid dilution effects by depositing many layers of the filler metal. The composition of the surface layer was designed to be Fe-0.234 wt.% C – 0.50% Mn – 0.28% Si – 1.70% Al – 0.02% Ni – 0.003% Ti – 0.006% O – 0.064 N. Stationary spot welds were produced on these bars to remelt and solidify the FCAW deposits using the gas-tungsten arc-welding (GTAW) process. The average welding power was maintained constant at 1.9 kW (110 A, 17.5 V, DCEN). Helium was used as the welding and shielding gas. In this work, two different welding conditions were used to vary the weld metal (WM) cooling rate. In the first experiment, the arc was extinguished at 17 s after initiation. This condition leads to rapid cooling of the weld. In the second experiment, the arc current was reduced in a slope-down mode from the peak current. This allowed the WM to cool slowly [see Fig. 1].

Results and Discussions

Rapidly cooled Welds: The TRXRD image representation of diffraction data from the HAZ and WM are presented in Fig. 2. In the HAZ region [see Fig. 2(*a*)], as soon as the arc was struck, peak position of ferrite (110) peak moved to the lower 2θ values indicating an increase in the lattice parameter due to thermal expansion. After 7 s, diffraction from austenite [fcc (111) peak] was observed. Continued weld heating led to an increase in austenite intensity and a decrease in ferrite intensity. After the arc was shut off (17 s), the austenite rapidly transformed to martensite, as shown by the decrease in austenite fcc (111) diffraction intensity and a corresponding increase in ferrite bcc (110) peak intensity. In addition, the persistence of ferrite at high temperature is evident from the intensity of bcc (110) diffraction peaks. This suggests that an increased amount of ferrite must be present at the HAZ. The result from the WM region is presented in Fig. 2(*b*). After the arc was extinguished, the liquid continued to exist as the only phase for an additional 0.2 s prior to the appearance of the austenite phase, as indicated by the fcc (111) peak. This result shows that austenite is the primary phase to solidify from the melt. As the weld cooled further, the austenite peaks shifted toward higher 2θ values, indicating a decrease in lattice spacing due to a drop in temperature. At about 3 s after the onset of solidification, ferrite was observed to coexist with the austenite, as indicated by the addition of the bcc (110) peak. Upon further cooling, the ferrite peaks also shifted toward higher 2θ values as the temperature approached ambient conditions. This result of primary austenite solidification was verified through repeated experiments.

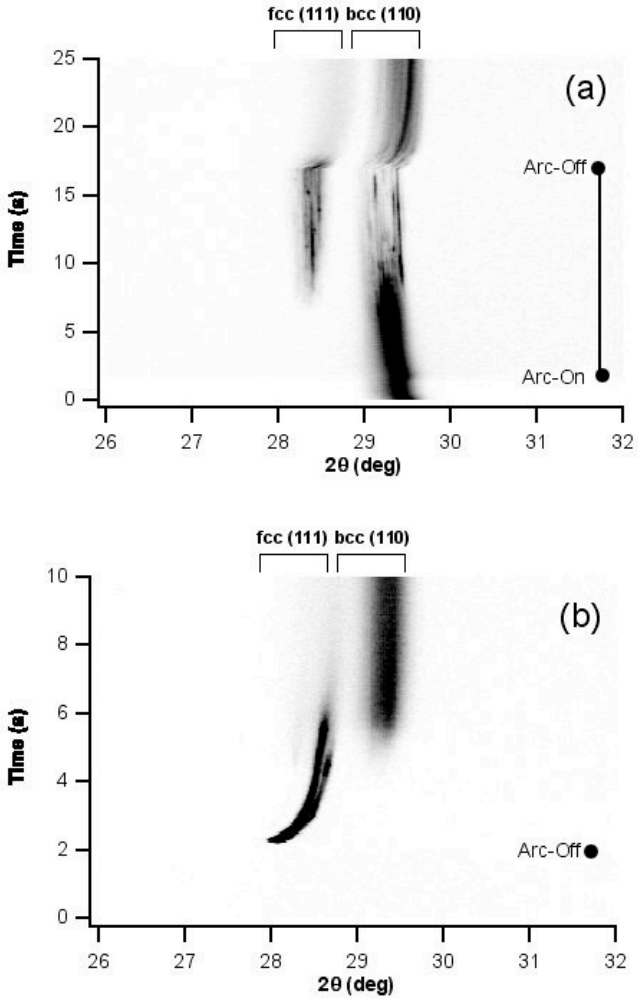

Fig. 2 Image representations of diffraction data from (*a*) the HAZ region and (*b*) the WM region from rapidly cooled weld. The high-intensity diffraction data are represented by black, background intensity by white. The arc-on and arc-off periods are shown.

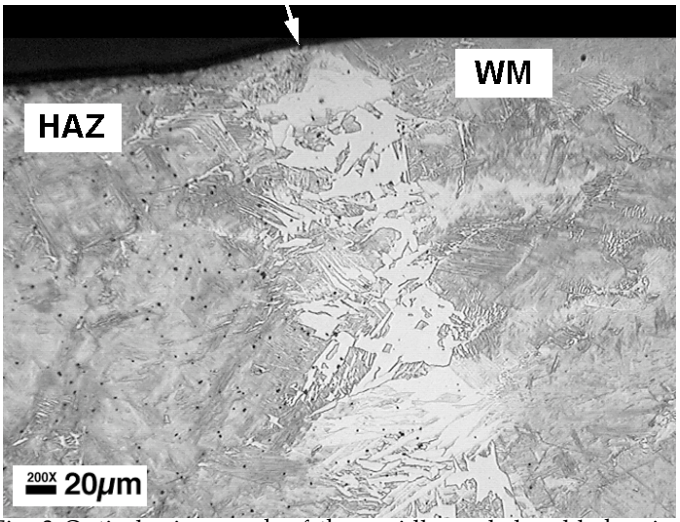

Fig. 3 Optical micrograph of the rapidly cooled weld showing the liquid-solid boundary through the absence of inclusions (indicated by white arrow).

Optical microscopy was performed on these stationary welds, and the micrographs are shown in Fig. 3. The micrograph shows the details of the HAZ and WM. The white region near the fusion line (marked by arrow) is identified as the δ-ferrite that formed at high temperature. The WM region contained only martensite with no columnar δ-ferrite microstructure confirming the TRXRD observation of austenite formation during weld cooling. Previous research has shown that, during a static welding experiment, the measured peak cooling rates are six times higher (~1500 Ks^{-1}) than the normal weld-cooling rates (~250 Ks^{-1}) [5]. Therefore, the observed transition from equilibrium ferrite to austenite solidification in current experiment is attributed to a change in weld-cooling rate.

Slow Cooled Welds: In the high cooling rate TRXRD experiment, the WM solidified with primary austenite, which is in contrast to the primary δ-ferrite solidification expected under normal slow cooling conditions. To evaluate the hypothesis that the mode change was brought about by an increase in the cooling rate, the weld current slope-down experiments were performed. Sloping down of welding current resulted a slower weld-cooling rate. The TRXRD measurements were obtained from the WM region [see Fig. 4].

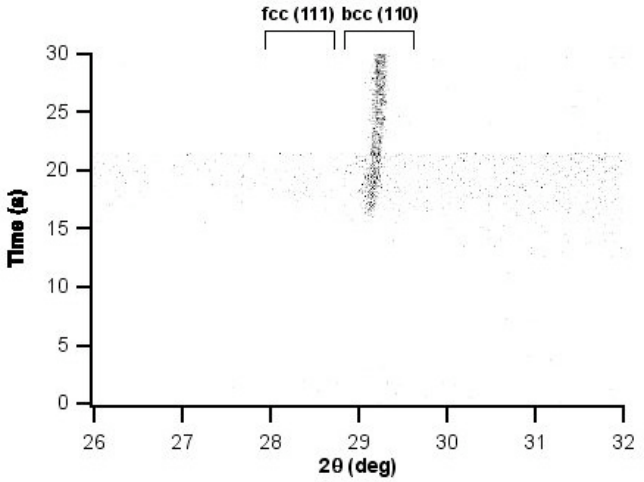

Fig. 4 TRXRD results from a slope-down experiment: showing the appearance of bcc (110) diffraction, first from the melt

In this result, for ~15 s after the slope down was started, only liquid was present and no diffraction from ferrite or austenite was evident. Continued decrease in welding current led to the appearance of bcc (110) diffraction peaks as the first solid phase. This confirmed the hypothesis that the reduced cooling rate would lead to ferrite primary solidification. To evaluate this solidification mode, optical microscopy was performed on the welds. The micrograph [see Fig. 5] shows an extended region of the ferrite phase as indicated by the large white region. An increase in ferrite thickness in this experiment is evident from the comparison of this micrograph with another micrograph taken at the same magnification from slow-cooled welds shown in Fig. 3. This observation indicates that the primary solidification in these regions occurs by ferrite formation and remains so compared to the switch to austenite mode of solidification that occurs in the rapid cool-down experiments.

Detailed observation of the microstructure to the right of this region also showed some interesting features. As mentioned earlier, as the welding current decreased further, below a certain welding current, the arc was extinguished. This leads to a rapid cooling toward the final stages of weld-solidification. The rapid cooling led to a transition from a primary ferrite mode of solidification to primary austenite mode. However, before this transition occurred, rapid changes in ferrite morphology take place.

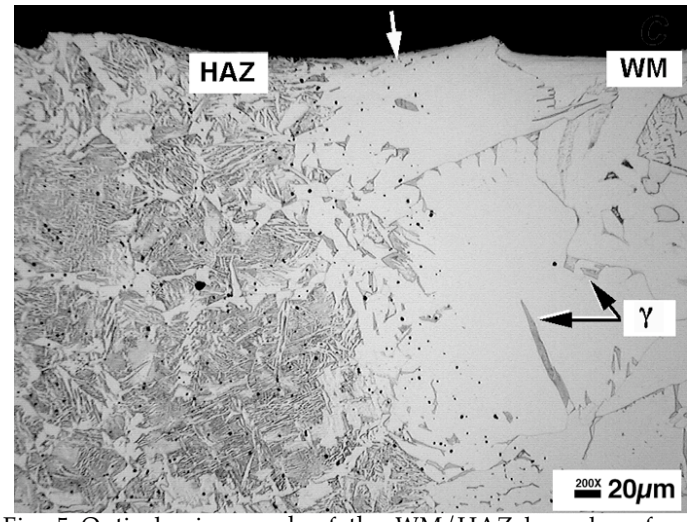

Fig. 5 Optical micrograph of the WM/HAZ boundary from slowly cooled weld showing the liquid-solid interface (marked by white arrow) inferred through the absence of inclusions and the regions of transformed austenite (marked as "G" within the ferrite blocks).

The above interpretation is consistent even with the observations based on the microstructural features in Fig. 3. In both cases shown in Figs. 3 and 5, the early stage of solidification occurs by the planar δ-ferrite solidification from the fusion line. In the case of the rapid cooling experiment, the transition to primary austenite solidification occurs very rapidly within ~20 μm of growth. However, in the slow-cooled weld, the primary ferrite solidification occurs for an extended time and leads to ~1000-μm-thick ferrite. This ferrite microstructure is typical of that observed in normal welding practice [1, 2].

Thermodynamic and Kinetic Calculations: The tendency for change in the primary solidification phase in Fe-C-Al-Mn alloys is evaluated by considering relative phase stability of ferrite and austenite with respect to liquid steel as a function of carbon and aluminum concentration at different temperatures. The liquid-ferrite and liquid-austenite phase equilibria as a function of aluminum concentration were calculated separately using ThermoCalc [6]. The results are shown in Figs. 6(*a* & *b*). The calculations for Fe-Al without carbon show the liquidus and solidus of ferrite phase are significantly higher than liquidus and solidus for austenite phase. This clearly indicates that austenite phase selections in Fe-Al alloys are thermodynamically not likely. In the case of Fe-Al-C-Mn alloys, the addition of carbon to the calculations

expanded both the liquid-ferrite and liquid-austenite phase equilibrium regions and it may be possible to obtain the transition from ferrite to austenite solidification in some of the Fe-C-Al-Mn steels by undercooling. To evaluate this hypothesis further, the extreme conditions of rapid solidification given by partitionless growth of ferrite or austenite growth from the liquid were evaluated by examining T_0 temperatures.

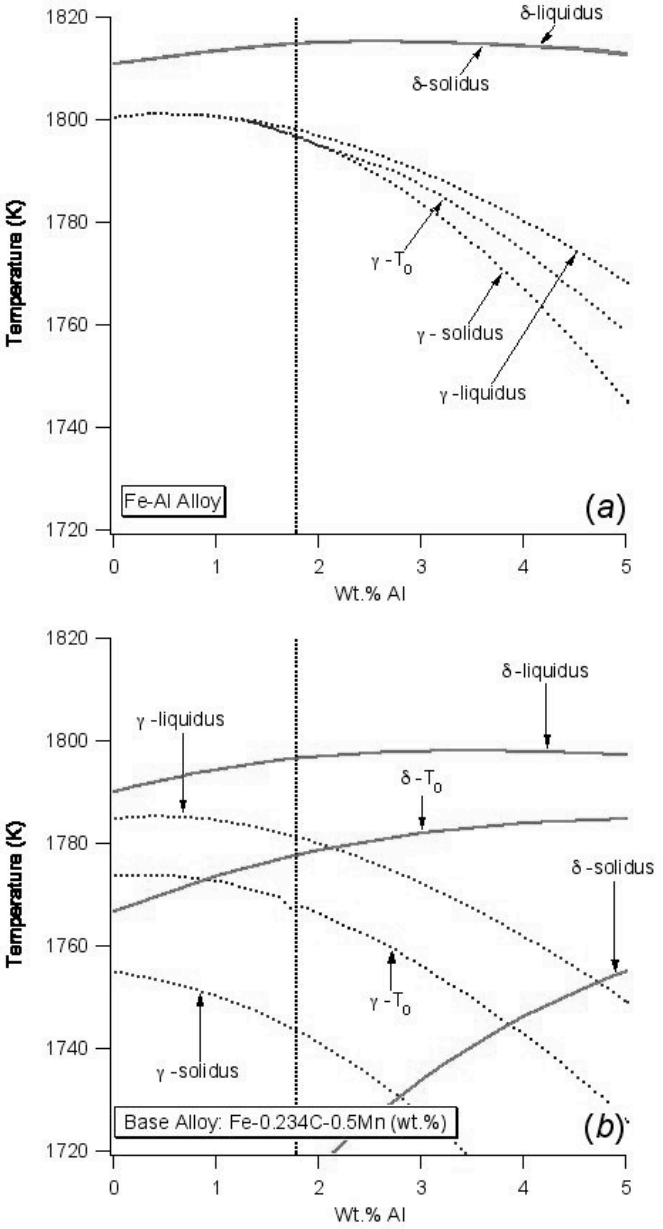

Fig. 6 Calculated liquid-ferrite and liquid-austenite phase equilibria as a function of aluminum concentration for (*a*) the Fe-Al system and (*b*) the Fe-Al-C-Mn system.

Interestingly, for the aluminum concentration of the present sample [at the vertical line in Fig. 6(b)], the T_0 line for ferrite is still above the T_0 line for the austenite. Therefore, even at large rapid cooling conditions, the direct formation of austenite during solidification is calculated to be less likely than that of ferrite. However, this speculation does not consider all of the dendrite growth parameters, such as the relationship between the velocity of the liquid-solid interface, the dendrite tip radius and the kinetic undercooling parameters that need to be analyzed with an interface response function model [7, 8, 9, and 10].

The interface response function model was applied to the Fe-C-Al-Mn system. Thermodynamic values were calculated using the TQ interface to ThermoCalc software [6]. For solving the interface response functions, the temperature gradient and interface velocity of solid-liquid interface is required. Experimental evaluations of these parameters are difficult due to the small size of the weld pool. However, these parameters can be obtained through numerical modeling. Recently, DebRoy and coworkers have used computational heat-transfer fluid flow models [11] to calculate the transient heating and cooling of a gas-tungsten arc spot weld under conditions similar to those in the present experiment. These calculations yield the following results: the maximum temperature gradient in liquid at the WM-HAZ boundary is 9×10^4 K/m, and the interface solidification growth velocity ranges from 5×10^{-3} to 1.5×10^{-2} m/s as the weld pool solidifies. These data were used for solving the solidification model to determine the dendrite tip temperatures for the austenite and ferrite phases. The results are plotted as a function of liquid-solid interface velocity in Fig. 7. The calculations show a sharp drop in dendrite tip temperature near to the planar interface instability at low interface velocities. As the velocity increases, the tip temperature increases and then starts decreasing above a critical value. The planar growth becomes stable again at the absolute stability limit (~0.5 ms^{-1}). The above changes were similar for ferrite and austenite solidification. The results show that for all the interface velocities, the dendrite tip temperature of ferrite is always higher than that that of austenite. The quantitative results from interface function models do not support the observed transition from equilibrium ferrite to nonequilibrium austenite solidification.

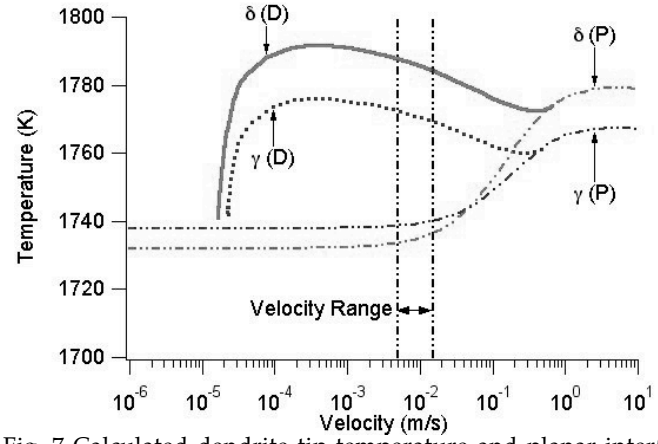

Fig. 7 Calculated dendrite tip temperature and planar interface temperature for ferrite and austenite solidification as a function of liquid-solid interface velocity.

Preliminary work considered the diffusion controlled dendritic growth of ferrite and austenite into liquid. The geometry of the simulation is shown in Fig. 8(*a*). The details of these calculations are given in reference 1. The

interface velocities of liquid-austenite and liquid-ferrite interface were calculated for a cooling rate of 500 K/s with DicTra software [12] for a constant interdendritic arm spacing of 200 μm. The results [see Fig. 8(*b*)] showed that as the weld cools, the velocity of liquid-austenite interface increases above that of liquid-ferrite interface at ~1764 K. This temperature corresponds to an undercooling of ~30 K below the equilibrium liquidus temperature of ferrite. This suggests that it is possible to grow austenite faster than ferrite, if the liquid-solid interface with austenite phase was undercooled. However, further work is necessary to evaluate such large undercooling.

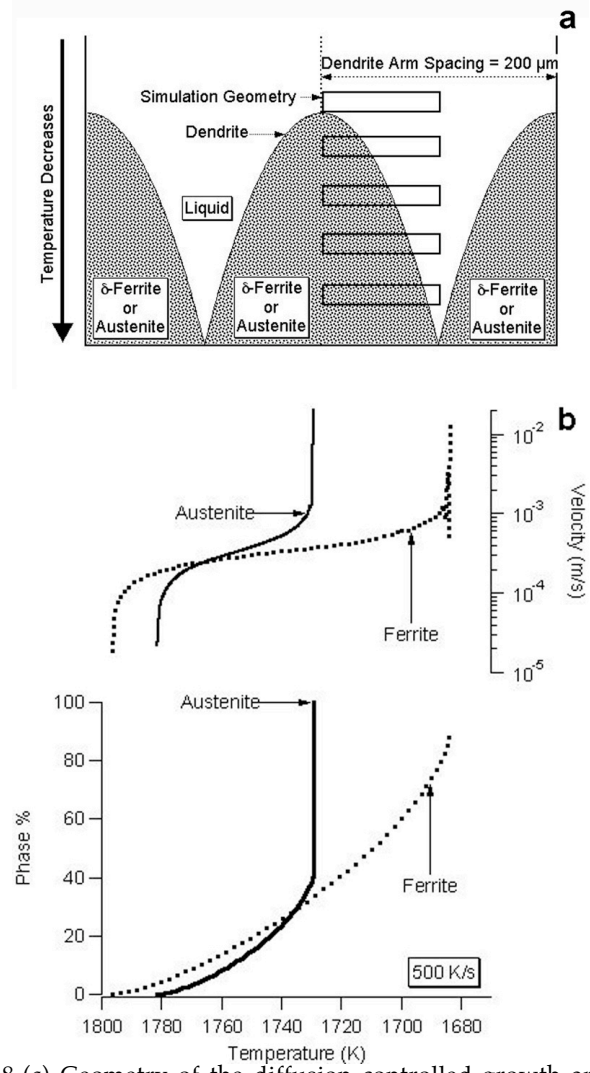

Fig. 8 (*a*) Geometry of the diffusion controlled growth and (*b*) calculated velocity of liquid-solid interface and phase fraction of ferrite (dotted line) and austenite (solid lines) as a function of temperature while cooling.

Summary and Conclusions

The TRXRD measurements from the HAZ region of a Fe-C-Al-Mn steel spot weld showed incomplete formation of austenite during the heating cycle and the presence of some ferrite even at the highest temperatures. During the cooling cycle, the austenite transformed to ferrite.

For the same conditions, the TRXRD results from the WM regions showed primary nonequilibrium austenite solidification. In contrast, primary ferrite solidification was observed in a slow cooled weld.

The dendrite tip temperature calculations did not support the observed transition from primary ferrite to austenite solidification. However, possibility of such transition at large undercooling was in qualitative agreement with computational thermodynamic and kinetic models.

Acknowledgements

This research was sponsored by the U.S. Department of Energy, Division of Materials Sciences and Engineering under contract No. DE-AC05-00OR22725 with UT-Battelle, LLC. A portion of this work was performed under the auspices of the U. S. Department of Energy, Lawrence Livermore National Laboratory, under Contract No. W-7405-ENG-48. The authors would like to thank Dr. J. Wong and Dr. T. Palmer of LLNL for help with the synchrotron diffraction experiments. In addition, we thank Prof. T. DebRoy for allowing us to use the unpublished results of heat- and mass-transfer calculations for gas-tungsten arc spot-welds.

References

1. S. S. Babu, S. A. David and M. A. Quintana, *Welding Journal*, 80, 91s-105s (2001)
2. M. A. Quintana, J. McLane, S. S. Babu, S. A. David, *Welding journal*, 80, 98s-105s (2001)
3. V. Karpenko, J. H. Kinney, S. Kulkarni, K. Neufel, C. Pope, K. G. Tirsell, J. Wong, J. Cernio, T. Troxel, and J. Yang, *Review of Scientific Instruments*, 60, 1451-1456 (1989)
4. J. W. Elmer, J. Wong and T. Ressler, *Scripta Materialia*, 43, 751-757, (2000)
5. S. S. Babu, J. W. Elmer, S. A. David and M. A. Quintana, *Proceedings of Mathematical, Physical and Engineering Sciences*, in press (2002)
6. B. Sundman, B. Jansson, and J. O. Andersson, *Calphad*, 9, 1- 153 (1985)
7. R. Trivedi, and W. Kurz, *International Materials Reviews*, **39**, 49-74 (1994)
8. S. Fukumoto and W. Kurz, *ISIJ International*, 37, 677-684 (1997)
9. S. Fukumoto and W. Kurz, *ISIJ International*, 38, 71-77 (1998)
10. S. Fukumoto and W. Kurz, *ISIJ International*, 39, 1270-1279 (1999)
11. W. Zhang, T. DebRoy and J. W. Elmer, Unpublished research, The Pennsylvania State University, State College, PA 16801, USA (2001)
12. A. Engström, L. Höglund, and J. Ågren, J. *Metall. Mater. Trans. A.*, 25A, 1127-1134 (1994)